Friction **11**(10): 1922–1938 (2023)
https://doi.org/10.1007/s40544-022-0730-6
ISSN 2223-7690
CN 10-1237/TH

RESEARCH ARTICLE

A modified model of Lundberg–Palmgren rolling contact fatigue formula considering the effects of surface treatments

Boyu ZHANG[1], Huaiju LIU[1,*], Peitang WEI[1], Mario GUAGLIANO[2], Shengwen HOU[3]

[1] *State Key Laboratory of Mechanical Transmissions, Chongqing University, Chongqing 400044, China*

[2] *Dept. Mechanical Engineering, Politecnico di Milano, Milano 20133, Italy*

[3] *Shaanxi Fast Auto Drive Refco Group Ltd., Xi'an 710119, China*

Received: 21 October 2022 / Revised: 18 November 2022 / Accepted: 05 December 2022

Abstract: The Lundberg–Palmgren (L–P) fatigue life formula, as a statistical fatigue theory, has been widely used in the industry. However, its direct applicability is limited to the components treated by surface strengthening technologies. Rolling contact fatigue tests and surface integrity measurements of American Iron and Steel Institute (AISI) 9310 rollers with several surface treatments were performed to address this issue. Based on these results, a modified L–P fatigue model was proposed, enabling the consideration of surface modification including surface roughness, residual stress, and hardening introduced by different surface treatments. Compared with the original L–P fatigue formula, its results are more accurate for surface strengthened specimens. Furthermore, this method can assess the contact fatigue life of gears treated by surface strengthening techniques.

Keywords: Lundberg–Palmgren (L–P) fatigue life formula; surface strengthening techniques; surface integrity; contact fatigue life assessment

1 Introduction

Since Weibull [1, 2] proposed fracture strength and fatigue life models, the statistical prediction method have been gradually applied in the industry. In 1947, based on American Iron and Steel Institute (AISI) 52100 bearing fatigue failure data, Lundberg and Palmgren [3, 4] developed a fatigue life model (Lundberg–Palmgren (L–P) fatigue model), which considered the relationship between the maximum orthogonal shear stress and the fatigue life. As a common statistical fatigue life model, the L–P fatigue model is constantly modified. Ioannides and Harris [5] introduced the fatigue-limiting shear stress to the original L–P fatigue model and put it forward in an integral form, which could be applied with the finite element method [6–8]. After that, Zaretsky [9] suggested that the Weibull distribution slope and the shear stress-life exponent should be taken into account independently. Until now, the L–P fatigue model and its modified models have been widely applied in the contact fatigue failure analysis [7, 10, 11]. In engineering practice, the International Standard Organization (ISO) 281 *Rolling bearings—Dynamic load ratings and rating life* [12], which applies the idea of L–P fatigue model, has been constantly updated and is widely accepted in the industry.

Surface strengthening technologies have been developed and widely used to increase the performance of load-carrying elements, such as gears and bearings. After those mechanical elements are treated by different surface strengthening technologies, their surface integrity parameters such as surface roughness, hardness, and residual stress were changed [13, 14]. Taking the shot peening process as an example, high-speed shot flow impacts the material surface

* Corresponding author: Huaiju LIU, E-mail: huaijuliu@cqu.edu.cn

Nomenclature

a	Half-width of Hertzian contact (m)
a_1, a_2	Surface integrity exponents, representing the effect of roughness
a_3	Surface integrity exponent, representing the effect of residual stress
a_4	Surface integrity exponent, representing the effect of surface hardness
A	Proportionality coefficient
c	Shear stress-life exponent
C_D	Dynamic load capacity (N)
d	Exponent (= 9)
e	Slope of the Weibull distribution
E	Young's modulus of specimen (Pa)
E_1	Young's modulus of driving specimen (Pa)
E_2	Young's modulus of driven specimen (Pa)
E^*	Equivalent young's modulus of specimen (Pa)
h	Depth–critical stress exponent
l	Length of the contact line (m)
L	Contact width (m)
m	Exponent (= 0.1)
N	Fatigue life (10^6)
N_{10}	Fatigue life with survival probability S of 10% (10^6)
N_{50}	Fatigue life with S of 50% (10^6)
$N_{50,E}$	Average experimental fatigue life (10^6)
$N_{50,LP}$	Predicted fatigue life from original L–P fatigue model (10^6)
$N_{50,MLP}$	Predicted fatigue life from modified L–P fatigue model (10^6)
p	Load-life exponent
P_d	Equivalent load (N)
P_H	Maximum Hertz contact pressure (Pa)
R_a	Surface roughness, arithmetic mean height of contour lines (μm)
R_1	Curvature radius of driving specimen (m)
R_2	Curvature radius of driven specimen (m)
R^*	Equivalent curvature radius (m)
S	Normalized probability of survival (%)
S_a	Surface roughness, arithmetic mean height of regional topography (μm)
S_q	Surface roughness, root mean square of regional topography (μm)
SH	Surface microhardness (HRC)
$SH_{grinding}$	Surface microhardness of grinding specimen (HRC)
V	Volume of the material stressed (m^3)
z_0	Depth of sub-surface maximum orthogonal shear stress (m)
σ_r	Residual stress at the depth of z_0 (Pa)
υ	Poisson's ratio
τ_0	Maximum orthogonal shear stress at sub-surface (Pa)
τ_{0r}	Sub-surface maximum orthogonal shear stress considering the effect of residual stress (Pa)
τ_{0s_a}	Sub-surface maximum orthogonal shear stress considering the effect of surface roughness (Pa)

continually, resulting in the refined material microstructure [15], the increased hardness [16], the residual compressive stress layer [17, 18], and the different surface micro-topography [19, 20]. Since these surface integrity parameters have a significant impact on fatigue life, the results of the original L–P fatigue model may be not sufficiently accurate for strengthened specimens and parts.

This work was devoted to developing of an advanced contact fatigue assessment model considering the surface modification. Carburized AISI 9310 rollers were manufactured as samples. These rollers were divided into nine groups and were treated by different surface strengthening methods including grinding (G), shot peening (SP), fine particle peening (FPP), and superfinishing (SF). Surface integrity parameter measurements and contact fatigue tests were carried out for all rollers. By fitting the experimental fatigue results to the original L–P fatigue model, empirical coefficients for rolling contact fatigue were obtained. A modified L–P fatigue model, which considers the surface integrity introduced by different surface treatments, was proposed. Compared with the original L–P formula, it resulted in more accurate fatigue life estimation for surface-enhanced elements. Finally, the ability of the proposed method to be applied to gear contact fatigue life assessment is discussed.

2 Experimental methods and results

2.1 AISI 9310 rollers and surface strengthening methods

The driving roller and the driven roller are shown in Fig. 1. The diameter of the outer circle of both driving roller and driven roller is 60 mm, their contact mode is line contact, and the contact width L is 3 mm. The specimen material was AISI 9310 steel, which is widely used in the aeronautics and automotive power trains. The Young's modulus E is 2.1×10^{11} Pa, and the Poisson's ratio υ is 0.3. Its chemical compositions are displayed in Table 1. All specimens initially underwent the same manufacturing process including rough turning, ultrasonic flaw detection, carburizing, thermal insulation, tempering, and grinding. The case-hardening layer depth of initial specimens was roughly 2 mm.

Different surface strengthening methods such as shot peening, fine particle peening, and superfinishing were adopted to the ground specimens. The strengthening processes are shown in Fig. 2. During shot peening, a pneumatic shot peening machine was adopted to some specimens, which consists of a shot incidence system, a nozzle movement system, an operating floor, a particle screening, a recovery system, a particle storage system, and a dedusting system. Meanwhile, some specimens were treated by fine particle peening with a fine particle peening machine. Compared with conventional shot peening

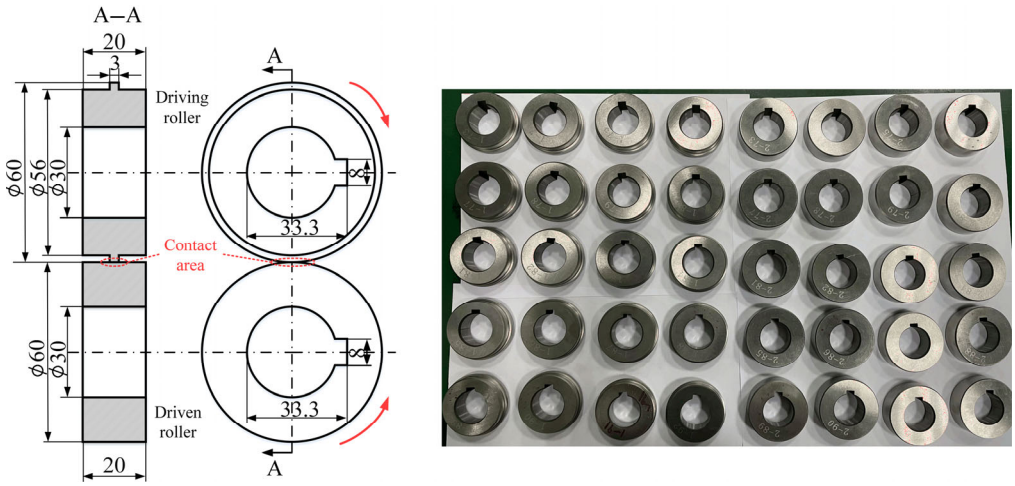

Fig. 1 Test specimens.

Table 1 Chemical compositions of AISI 9310 (wt%).

C	Si	Mn	P	S	Cr	Mo	Ni	Cu	B
0.07–0.13	0.15–0.35	0.4–0.7	≤ 0.015	≤ 0.015	1.0–1.4	0.08–0.15	3–3.5	≤ 0.35	≤ 0.001

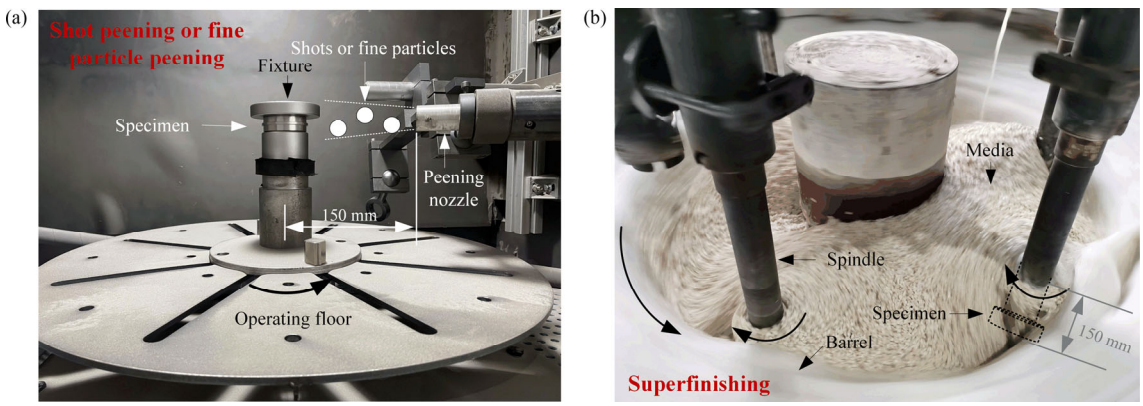

Fig. 2 Strengthening processes of specimens: (a) shot peening or fine particle peening equipment and (b) superfinishing equipment.

machine, it has a higher air pressure. Table 2 represents the processes of shot peening and fine particle peening. Additionally, some ground specimens and shot-peened specimens were superfinished by a vertical spindle barrel finishing machine to represent a "mirror-like" surface state. During the superfinishing process, clockwise rotation and anticlockwise rotation of spindle and barrel took the equal amount of time. The superfinishing process parameters can be seen in Table 3.

2.2 Surface integrity measurement and results

The surface roughness, residual stress gradient, and microhardness gradient of specimens before and after surface treatments were measured to characterize the surface integrity state. As there is just a small difference between the driving and driven rollers after the same surface strengthening process, only the measurement results of the driving rollers are given.

The surface micro-topography was measured by a white light interferometer (MFT-5000, Rtec). Some measured surface micro-topographies are illustrated in Fig. 3. Then the average values of areal surface roughness S_a (arithmetic mean height of regional topography) and S_q (root mean square of regional topography) for each surface treatment were calculated, as listed in Table 4.

The X-ray portable diffractometer (μ-360s, PULSTEC) for residual stress measurement was implemented. This instrument works according to the two-dimensional cosα measuring principle [21]. To obtain the in-depth residual stress gradient, the electrolytic polishing machine (8818-V2, Proto) and the electrolyte (saturated sodium chloride solution) were adopted to corrode the specimens to the wanted depth. The corrosion depth was measured by a digital display micrometer with the accuracy of 1 μm. The residual stress at each material point was tested 3 times, and those values were averaged as the final residual stress. Since the values of the axial residual stress and hoop residual stress of SP, FPP, and SF are not very different [22–24], only the axial residual stress gradients are given in Fig. 4(a). When the depth is greater than 0.1 mm, the residual compressive stress of the G, FPP, and SF-30 min specimens equal to about −270 MPa.

For observing the microhardness gradient of specimens, the specimens were cut and inlaid firstly. Then the microhardness at different depths were measured by a digital display automatic rotary microhardness tester (MHVS-1000AT, Shanghai Aolong Xingdi Testing Equipment Co., Ltd.). The loading force was 0.5 N, and the load holding time was 10 s. The test results of microhardness are displayed in Fig. 4(b).

2.3 Rolling contact fatigue tests and results

Rolling contact fatigue tests were conducted for specimens with different surface treatments. A rolling contact fatigue testing machine (CQHH-RCF-A,

Table 2 Parameters for shot peening (SP) and fine particle peening (FPP).

	Import angle (°)	Import distance (mm)	Shot			Almen Intensity	Coverage rate
			Material	Diameter (mm)	Hardness (HRC)		
SP	90	150	Steel cut wire shot	0.6	55–62	0.20 mmA	200%
	90	150	Steel cut wire shot	0.6	55–62	0.35 mmA	200%
	90	150	Steel cut wire shot	0.6	55–62	0.50 mmA	200%
FPP	90	150	High-speed steel shot	0.05	70	0.05 mmN	200%
	90	150	High-speed steel shot	0.05	70	0.10 mmN	200%
	90	150	High-speed steel shot	0.05	70	0.15 mmN	200%

Table 3 Superfinishing process parameters.

Initial state of specimen	Spindle rotation speed (r/min)	Barrel rotation speed (r/min)	Embedded depth of specimen (mm)	Time of duration (min)	Mill
G	147	47	150	30	White corundum TP3×3
SP-0.35 mmA	147	47	150	30	White corundum TP3×3

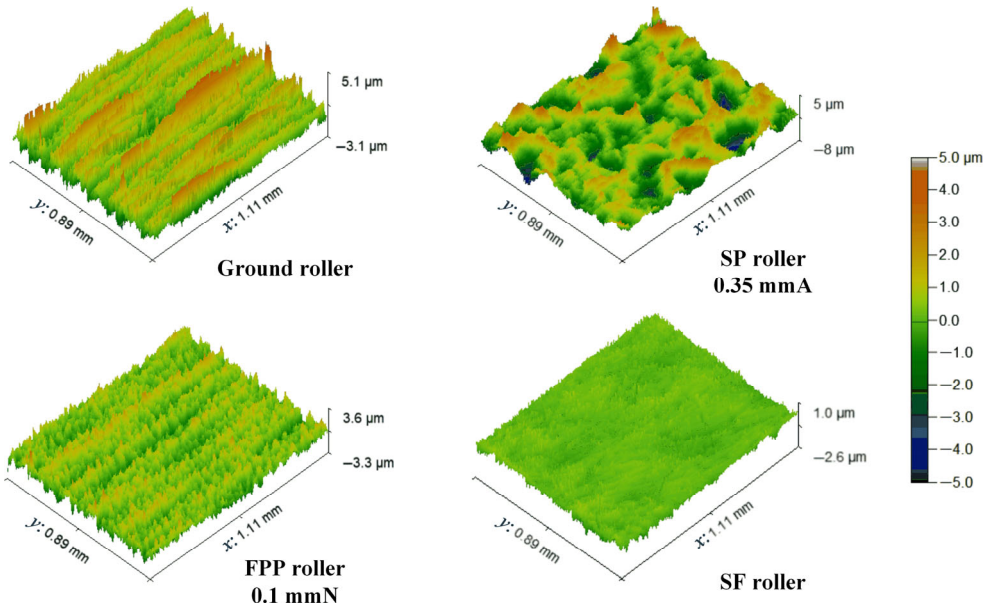

Fig. 3 Typical surface micro-topographies.

Table 4 Surface roughness of different surface treatments.

Specimen	S_a (μm)	S_q (μm)
G	0.68	0.86
SP-0.2 mmA	0.81	1.06
SP-0.35 mmA	0.88	1.15
SP-0.5 mmA	0.96	1.24
FPP-0.05 mmN	0.33	0.42
FPP-0.1 mmN	0.50	0.55
FPP-0.15 mmN	0.53	0.65
SF-30 min	0.13	0.18
SP-0.35 mmA + SF-30 min	0.14	0.19

Chongqing University of Technology) was used, which primarily consists of a test system, a lubrication and cooling system, a control system, and a machine vision system. It can detect fatigue failure in real-time through the machine vision technology, enabling automatic shut-down once the failure threshold achieves. When the area of micro-pitting reached 15% within 10 mm^2, or the pitting area was no less than 3 mm^2, the specimen was judged to have fatigue failure. If the cycle number of the specimen exceeded 10^7, the fatigue life of the specimen was considered to leap out of the experimental range (run-out). The rolling contact fatigue tester is illustrated in Fig. 5.

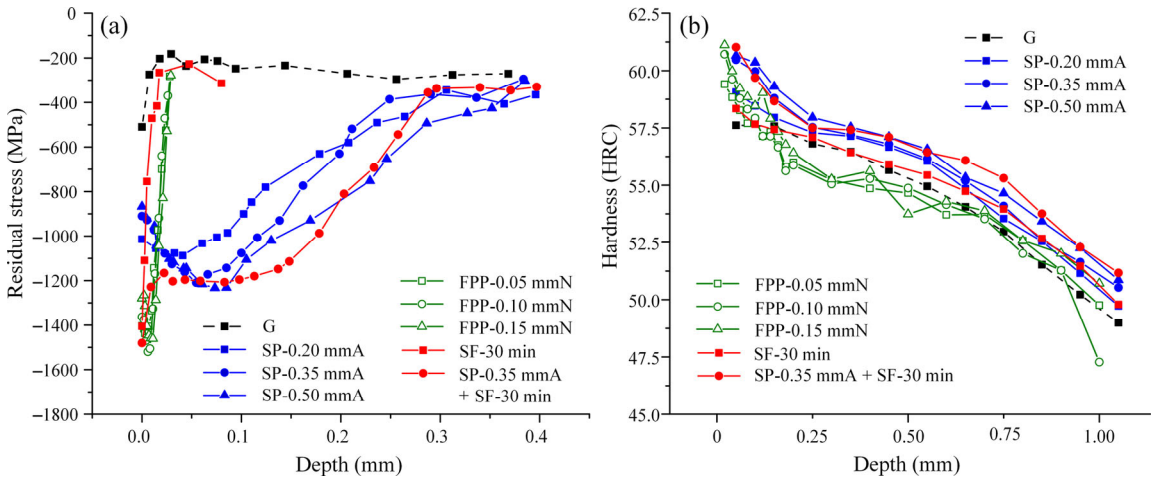

Fig. 4 (a) Residual stress gradient after surface treatments and (b) microhardness after surface treatments.

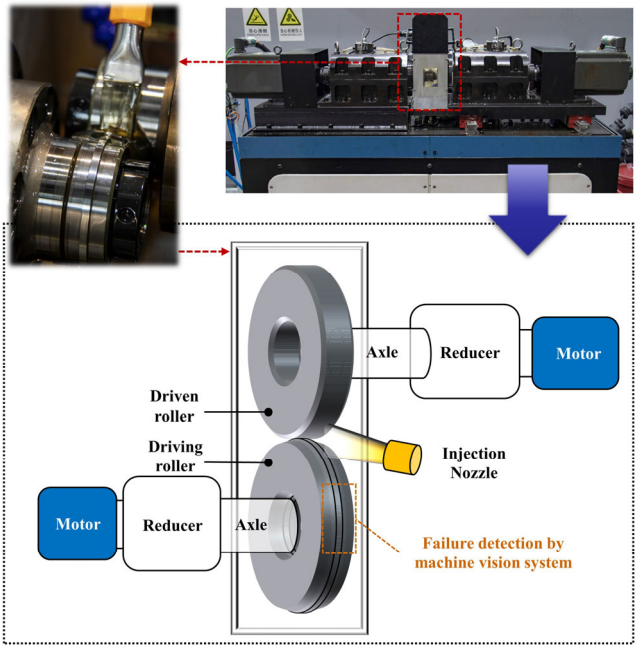

Fig. 5 Rolling contact fatigue tester.

The rotating speed of driving roller was set at 1,600 r/min, and the rotating speed of driven roller was 1,760 r/min. The slip ratio was controlled as 10% to simulate gear drive. The jetted lubricating oil was a commercial industrial lubricant (600 XP100, Mobil). The ground specimens were subjected to the maximum Hertz contact stress of 2,500, 2,750, and 3,000 MPa. There were at least 5 test points under each loading level, which were averaged as the final fatigue life under this loading level. The other strengthened specimens were first subjected to 2,500 MPa stress loading. If the fatigue lives of all specimens of a certain strengthening process exceeded 10^7, the load increased to 3,000 MPa. The experimental results of rolling contact fatigue of different surface treatments are shown in Table 5. The failure pictures of some rollers are shown in Fig. 6. Except for one FPP-0.15 mmN roller, which was judged to fail due to excessive vibration, the rest of the specimens suffered pitting failure.

Table 5 Experimental results of rolling contact fatigue of AISI 9310 rollers.

Specimen	Maximum Hertz contact pressure P_H (MPa)	Average experimental fatigue life $N_{50,E}$ (10^6)	Standard deviation (10^6)
G	2,500	4.601	0.814
G	2,750	1.762	0.257
G	3,000	1.010	0.097
SP-0.2 mmA	2,500	4.829	2.266
SP-0.35 mmA	2,500	5.861	1.258
SP-0.5 mmA	2,500	5.509	3.268
FPP-0.05 mmN	2,500	10.000 (run-out)	—
FPP-0.05 mmN	3,000	1.782	0.555
FPP-0.1 mmN	2,500	6.688	1.159
FPP-0.15 mmN	2,500	7.809	2.786
SF-30 min	2,500	10.000 (run-out)	—
SF-30 min	3,000	2.520	3.119
SP-0.35 mmA+SF-30 min	3,000	3.202	0.731

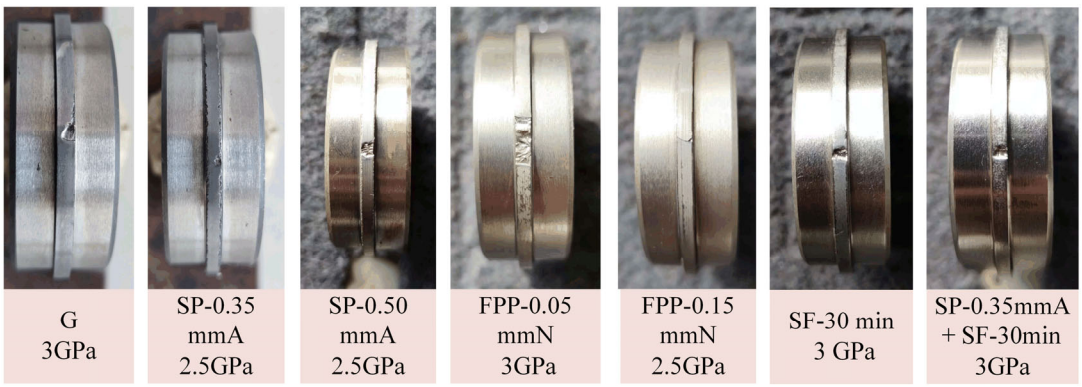

Fig. 6 Failure of some rollers after rolling contact tests.

3 L–P fatigue model and results

3.1 L–P fatigue model

Among the many fatigue life models depended on statistical data, the L–P fatigue model was the first widely accepted and used in Ref. [12]. After a statistical analysis of abundant experimental AISI 52100 bearing fatigue life, Lundberg [3, 25] and Palmgren [26] proposed a classical bearing fatigue life prediction model on the basis of two-parameter Weibull distribution [1, 2] for the first time. They related the bearing fatigue life N to the maximum orthogonal shear stress τ_0 at sub-surface, the depth of sub-surface maximum orthogonal shear stress z_0, and the volume of the material stressed V. The L–P fatigue model can be represented as

$$\ln\frac{1}{S} \propto \frac{\tau_0^c N^e V}{z_0^h} \tag{1}$$

where S is normalized to the probability of survival. If S is equal to 10%, the fatigue life can be expressed as N_{10}, which are widely used to predict the fatigue life of bearings and gears. While the fatigue life N_{50} with probability of survival S = 50% can be regarded as the average fatigue life. e is the slope of the Weibull distribution, indicating the of dispersion degree of data. c represents the shear stress-life exponent, and h represents the depth–critical stress exponent. The empirical constants c, h, and e can be determined from the experimental bearing fatigue life data. The L–P fatigue model can also be expressed as

$$N = \left(\frac{C_D}{P_d}\right)^p \tag{2}$$

where C_D is the dynamic load capacity, which can be calculated according to the material characteristics and geometric parameters [26], P_d is the equivalent load, and p is the load-life exponent. Afterwards, there are many modified formulas from Eq. (2), such as Zaretsky's formulae [27–30].

The fatigue life with S = 50% was adopted to present the roller fatigue life N_{50}, which can be expressed as

$$N_{50} = A\left(\frac{\ln\frac{1}{0.5}z_0^h}{\tau_0^c V}\right)^{1/e} \tag{3}$$

where A represents the proportionality coefficient, affected by material properties, and can be determined from the fatigue experiment.

The τ_0, z_0, and V can be calculated by Eqs. (4)–(6) [31]:

$$\tau_0 = 0.25P_H \tag{4}$$

$$z_0 = 0.5a \tag{5}$$

$$V = lLz_0 \tag{6}$$

where P_H is the maximum Hertz contact pressure, a is the half-width of Hertzian contact area, which can be calculated by Hertz contact formula [32], as demonstrated in Fig. 7, L is the contact width, and l is the length of the contact line, equaling to the circumference of the roller.

3.2 Predicted results of L–P fatigue model

The empirical constants c, h, and e can be derived by fitting the experimental bearing fatigue life data to the model. According to the experimental data of AISI 52100 bearing life, it is suggested that the empirical constants e = 1.11, c = 10.33, and h = 2.33 were for point contact, and e = 1.125, c =10.33, and h = 2.33

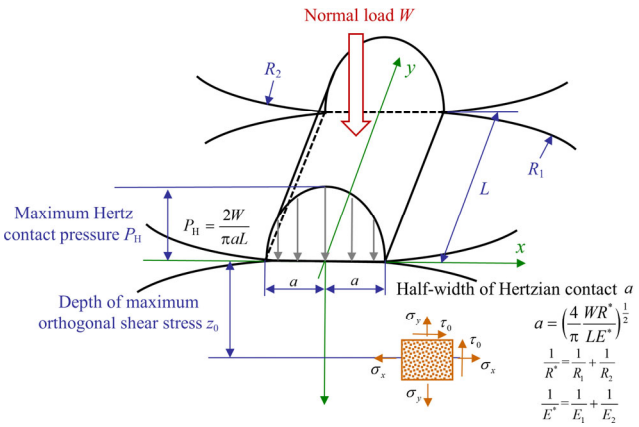

Fig. 7 Hertz contact pressure distribution of rollers. Note: R_1, R_2, and R^* are the curvature radius of driving specimen, curvature radius of driven specimen, and equivalent curvature radius, respectively; and E_1, E_2, and E^* are the Young's modulus of driving specimen, Young's modulus of driven specimen, and equivalent Young's modulus of specimen, respectively.

were for line contact [3]. While in the National Aeronautics and Space Administration (NASA), USA, fatigue tests of AIS1 9310 steel spur gears, e = 3, c = 10.33, and h = 2.33 were determined [33]. Soon after, the e for AIS1 9310 steel spur gears was revised by NASA to 2.5 [34]. Therefore, in this work, the empirical constants e = 2.5 and h = 2.33 were decided for AIS1 9310 steel rollers.

In terms of c and A, Townsend et al. [34, 35] pointed out that c could reach more than 23 by deriving from p and e. While Zaretsky [9] found that the most c varied from 6 to 12 in a lot of literatures about rolling contact fatigue. Therefore, for determining c and A, we fitted the experimental fatigue lives of ground rollers under three different loads to the L–P fatigue model by the multiple nonlinear regression method. Then c and A were determined as 17.57 and 1.12×10^{63}, respectively. The fatigue life of AIS1 9310 steel rollers with S = 50% can be represented as

$$N_{50} = 1.12\times10^{63}\left(\frac{\ln\dfrac{1}{0.5}z_0^{2.33}}{\tau_0^{17.57}V}\right)^{1/2.5} \tag{7}$$

The experimental and simulated fatigue lives of ground rollers under different loads are displayed in Fig. 8. It can be seen that the simulated and experimental fatigue lives of all rollers are very similar. When P_H = 2,500, 2,750 and 3,000 MPa, the absolute errors are 10.932%, 24.801%, and 23.762%, respectively. The predicted fatigue lives under P_H = 2,750 and 3,000 MPa are slightly higher than their experimental fatigue lives, while the value for P_H = 2,500 MPa (Fig. 8) is marginally lower than its experimental fatigue life. The errors are generally acceptable for fatigue life assessment [36–38].

When Eq. (7) is applied to all roller specimens, the predicted results are shown in Fig. 9. It can be found that the L–P fatigue model (Eq. (7)) can predict the fatigue life of the initial grinding specimen and shot peening specimen accurately. While for the most specimens treated by fine particle peening, the error in the predicted fatigue life was less than that in the double error band, compared with the experimental results. Nonetheless, the L–P fatigue model significantly underestimated the fatigue life of specimens after superfinishing. This means that the L–P fatigue model

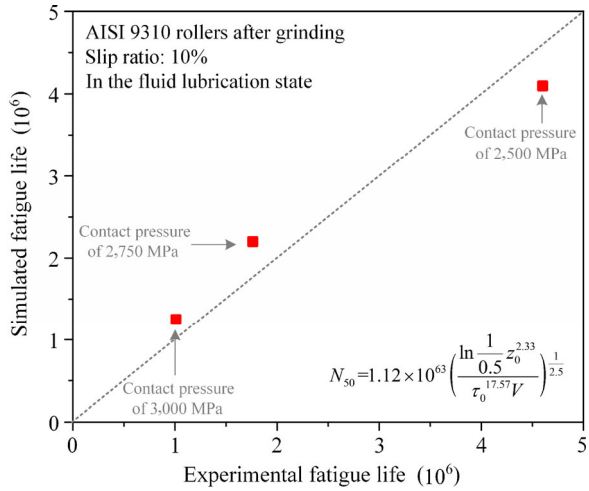

Fig. 8 Comparison of experimental and simulated fatigue lives of ground rollers under different loads.

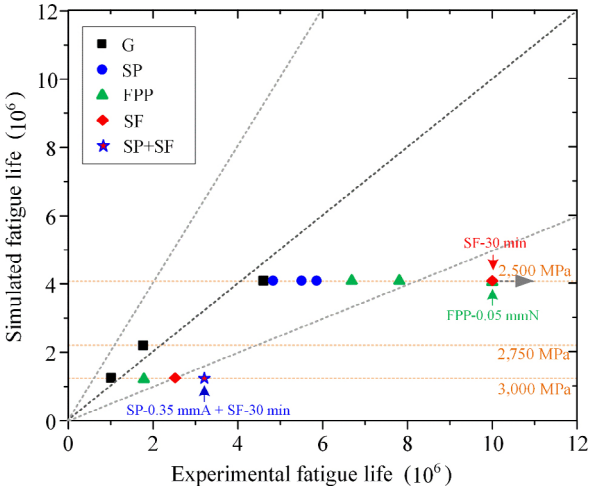

Fig. 9 Comparison of experimental and simulated fatigue lives of AISI 9310 rollers.

has poor applicability for the parts after surface strengthening, especially the parts with good surface condition.

Since the application of SF is gradually popularized, especially in bearing parts such as gear, it is necessary to consider the surface integrity parameters introduced by surface strengthening in the model.

4 Modified L–P fatigue model and results

4.1 Modified L–P fatigue model

Since the L–P fatigue model does not consider the surface integrity factors and their quality, a modified model was developed for aiming to quantitatively take

into account the surface hardness, surface roughness, and residual stress.

Indeed, there are many high-quality discussions and proposals regarding the effect of hardness gradient on contact fatigue life. Choi and Liu [39] built a crack initiation and propagation life model taking into account the hardness gradient characteristics, and found that the micro-hardness yields less than a change of 20% in both the crack initiation life and the crack propagation life. Walvekar and Sadeghi [40] proposed a finite element model considering hardness gradient of carburized 8620 steel, and deduced correction factor of the fatigue life N_{10} to obtain the optimal depth of hardening layer under different loads. Wang et al. [41] established the elastic–plastic finite element model of contact fatigue failure of carburized gear based on Dang van criterion, and thought that the risk of contact fatigue failure would decrease with the increase of hardened layer depth or the decrease of surface hardness.

However, the effect of hardened layer depth was not discussed in this paper since the hardened layer depth introduced by surface strengthening technologies, such as shot peening, did not exceed that of initial carburized AISI 9310 rollers. In addition, the effect of surface hardness on the fatigue life was proposed to be expressed in the form of $\exp(m(SH-a_4))$ by Zaretsky et al. [28, 29, 42], which has been adopted by Ref. [12]. The constant m equals to 0.1, SH is the surface hardness, and a_4 is the surface hardness of standard specimens (ground roller, 57.5 HRC). Figure 10 illustrates the relationship between $N_{50,E}$ and surface hardness under P_H = 2,500 MPa according to the Zaretsky's method. It can be found that except for the SF-30 min and FPP-0.05 mmN specimens, other scatters generally distribute around the curve of $N_{50,E} = N_{50,E,grinding}\exp(0.1(SH-SH_{grinding}))$. The fatigue lives of specimens after superfinishing or fine particle peening may greatly increase due to good surface condition, compared with those of other specimens. Therefore, the predicted results by this method are deemed to be consistent with our experimental results, and the hardness effect term $\exp(0.1(SH-57.5))$ is adopted to modify the L–P fatigue model.

The effect of surface roughness on contact fatigue life has been the focus of many scholars. It is generally believed that the contact fatigue life decreased with

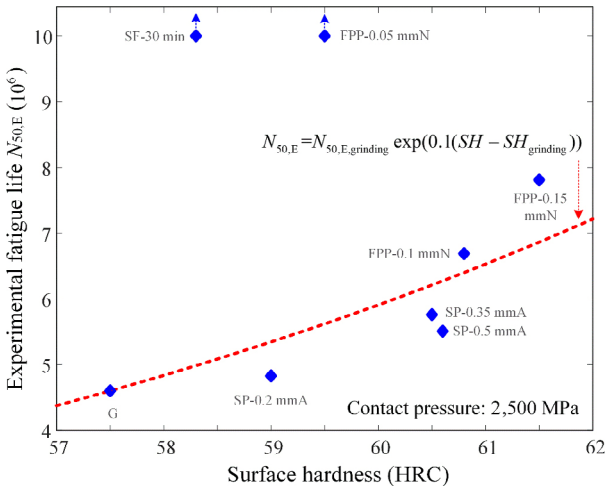

Fig. 10 $N_{50,E}$–SH relation under 2,500 MPa.

the increasing roughness [43–45]. In addition, surface roughness also affects fatigue failure modes. Sub-surface-initiated contact fatigue failure occurs when the surface roughness is small, while surface-initiated failure appears as the stress concentration near the surface caused by roughness is more prominent [46–48]. By introducing a function to describe near-surface failure caused by roughness, Morales-Espejel et al. [49] successfully modified the L–P fatigue life model to consider the competitive failure mechanism between surface and sub-surface of bearings. However, this complex formula was not used in engineering practice. Although in Ref. [12] the influence of lubrication state and surface roughness on fatigue life could be considered, its empirical coefficients, obtained from the bearings, might not suit rollers and gears.

In this paper, the fluid film lubrication state was constantly maintained during these contact fatigue experiments. So the effect of the lubrication state is not explored. Due to friction and slip rate, the height of roughness peaks of the rollers gradually decreased, and the surface micro-topography slowly became smooth with the growth of the cycle number. After that, most of rollers experienced sub-surface failure, which can be seen in Fig. 6. Therefore, it is quite appropriate to adopt the L–P fatigue life model to these rollers. Since S_a has little influence on z_0 and V, the effects are ignored. However, some literatures manifested that the surface roughness changed the stress distribution at sub-surface [50], and increased the sub-surface maximum orthogonal shear stress, especially in the film lubrication [51, 52]. Therefore,

the influence of the surface roughness on the τ_0 is only considered. The relationship $\tau_{0s_a} = \tau_0(a_1 S_a + a_2)$ is assumed to represent the effect of surface roughness on the maximum orthogonal shear stress (where a_1 and a_2 are the surface integrity exponents), and its coefficients are still to be determined.

The methods, introducing the residual stress to the fatigue model, have been widely considered by many researchers. In most methods, residual stress has been transformed into a certain stress, which relates with the fatigue life. Zaretsky et al. [27] and Townsend and Zaretsky [53] combined the residual stress with the principal stress to discuss its influence on fatigue life. To be explicit, the residual stress at z_0 was multiplied by a coefficient of 0.5 and added to the maximum shear stress. Agha [54] introduced the residual stress to the von Mises stress criterion, which could be applied to predict the maximum von Mises stress and its depth, and then calculate the fatigue life. Bernasconi et al. [55] assumed that the residual stress only affected the hydrostatic stress term when Dang Van criterion was applied to analyze rolling contact fatigue behavior of wheels. Wang et al. [56] established an elastic–plastic contact fatigue finite element model by adding the residual stress gradient to the pre-stressed field. When L–P fatigue model is applied, residual stress is expected to be added to the maximum orthogonal shear stress. Until now, no literature illustrates the relationship between the introduced residual stress and the τ_0. In reference to the thought of Zaretsky et al. [27], the residual stress σ_r at z_0 is multiplied by a coefficient a_3, and then added the τ_0. Therefore, the maximum orthogonal shear stress combined with residual stress can be represented as the equation of $\tau_{0r} = \tau_0 + a_3\sigma_r$, and the coefficient a_3 will be determined by the multiple nonlinear regression method later.

To sum up, the modified L–P fatigue life model considering surface integrity can be expressed as

$$N_{50} = 1.12\times10^{63}\left\{\frac{\ln\dfrac{1}{0.5}z_0^{2.33}}{[\tau_0(a_1S_a+a_2)+a_3\sigma_r]^{17.57}V}\right\}^{1/2.5}\cdot\exp(m(SH-a_4)) \tag{8}$$

where N_{50} represents the fatigue life with S = 50%, S_a is the surface roughness, SH is the surface hardness, and σ_r is the residual stress at the depth of z_0. m (= 0.1) is an exponent, and the surface hardness of standard specimens a_4 is equal to 57.5 HRC. The coefficients a_1, a_2 and a_3 will be calculated by the multiple nonlinear regression method later.

Table 6 summarizes the measured results, which are involved into Eq. (8). For fine particle peening and superfinishing, the depth of residual stress layer introduced is much less than z_0, and the residual stress value is the same as the value of ground rollers

Table 6 Measured results of surface integrity.

Specimen	P_H (10^6 Pa)	S_a (μm)	SH (HRC)	z_0 (10^{-4} m)	σ_r (10^6 Pa)
G	2,500	0.68	57.5	3.26	−270
G	2,750	0.68	57.5	3.57	−270
G	3,000	0.68	57.5	3.90	−270
SP-0.2 mmA	2,500	0.81	59.0	3.26	−310
SP-0.35 mmA	2,500	0.88	60.5	3.26	−363
SP-0.5 mmA	2,500	0.96	60.6	3.26	−448
FPP-0.05 mmN	2,500	0.33	59.5	3.26	−270
FPP-0.05 mmN	3,000	0.33	59.5	3.90	−270
FPP-0.1 mmN	2,500	0.50	60.8	3.26	−270
FPP-0.15 mmN	2,500	0.53	61.5	3.26	−270
SF-30 min	2,500	0.13	58.3	3.26	−270
SF-30 min	3,000	0.13	58.3	3.90	−270
SP-0.35 mmA + SF-30 min	3,000	0.14	61.5	3.90	−330

at z_0, which can be seen in Fig. 4(a). Hence the same residual stress value (−270×10^6 Pa) is applied for specimens treated by grinding, fine particle peening, and superfinishing. After that, the multiple nonlinear regression method is adopted to solve the coefficients a_1, a_2 and a_3.

The coefficients are calculated as $a_1 = 0.1757$, $a_2 = 1.0060$, and $a_3 = 0.2869$.

For AISI 9310 rollers, the modified L–P fatigue model can be expressed as

$$N_{50} = 1.12\times10^{63}\left\{\frac{\ln\frac{1}{0.5}z_0^{2.33}}{[\tau_0(0.1757S_a+1.006)+0.2869\sigma_r]^{17.57}V}\right\}^{1/2.5}\cdot\exp(0.1(SH-57.5)) \tag{9}$$

It should be noted that this modified formula can be applied to the carburized rollers with the similar material properties to AISI 9310. And fluid lubrication state needs to be guaranteed. This formula is more suitable for the case when the surface roughness S_a does not exceed 1 μm, and the failure occurs at sub-surface. The surface roughness R_a can replace S_a if no measurement equipment or condition for areal measurement is available [57, 58].

4.2 Modified L–P fatigue model results

The scatter diagram of $N_{50,E}$ and the predicted results of the original L–P fatigue model (Eq. (7)) and modified L–P fatigue model (Eq. (9)) are displayed in Fig. 11. Compared with the gray scatters, which refer to the L–P model, the colored scatters, which refer to the modified L–P model, are closer to the line of $y = x$. From the original L–P model, the predicted results of the specimens strengthened by FPP-0.05 mmN, SF-30 min, and SP-0.35 mmA + SF-30 min are less than half of these experimental results. In contrast, after the modification, the errors in the predicted fatigue life were less than that in the 1.5 time of error band, compared with the experimental results.

Table 7 gives some detail of predicted fatigue life in terms of the error. The $N_{50,E}$ represents the average experimental fatigue life. The $N_{50,LP}$ and $N_{50,MLP}$ are the predicted fatigue lives from the original and modified L–P fatigue model, respectively. It can be found that the absolute errors of the original formula are 10.932%–60.962%, whereas the absolute error of the modified L–P fatigue model is less than 26.520%. There is no doubt that the modified L–P fatigue model is more accurate and suitable for predicting the fatigue life of rollers after being strengthened.

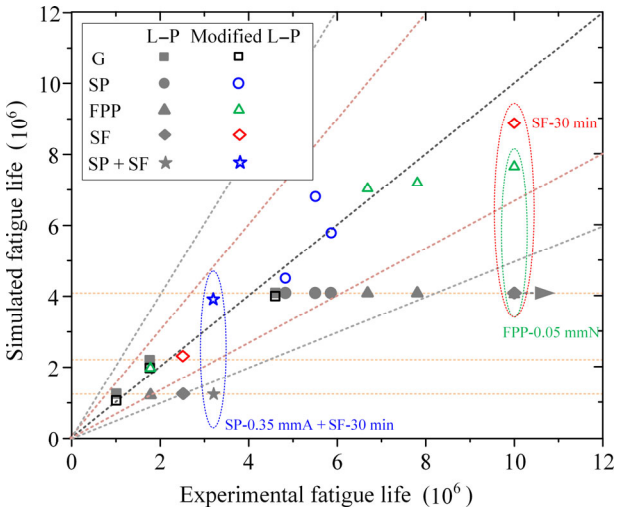

Fig. 11 Simulated fatigue lives of AISI 9310 rollers.

4.3 Effect of single factor

If only one factor is considered, the predicted results of the modified formula under contact pressure of 2,500 MPa are shown in Figs. 12(a)–12(c). Fatigue life experiences a significant increase with the growth of the surface hardness. It can be observed from Table 7 that the predicted fatigue life of the original $N_{50,LP}$ under this load is 4.098×10^6. When the surface hardness reaches 64 HRC, the fatigue life will be approximately 8×10^6, which is about twice as $N_{50,LP}$. Meanwhile, a dramatic decline can be observed in the fatigue life with the increase of the surface roughness. If the surface roughness exceeds 1.0 μm, the fatigue life of roller may be below 1.3×10^6. Additionally, residual compressive stress also has a positive effect on fatigue life. The average fatigue life of specimen will arrive at nearly 17×10^6 if the smooth standard specimens have the residual compressive stress of −400 MPa at the maximum orthogonal shear stress depth.

Figure 12(d) illustrates three contour surfaces with fatigue lives of 1×10^6, 10×10^6, and 100×10^6 under a contact pressure of 2,500 MPa. The specimens with higher surface hardness, smaller surface roughness, and

Table 7 Prediction results of the modified and original L–P fatigue model.

Specimen	Contact pressure (MPa)	$N_{50,E}$ (10^6)	$N_{50,LP}$ (10^6)	Absolute error of original L–P model (%)	$N_{50,MLP}$ (10^6)	Absolute error of modified L–P model (%)
G	2,500	4.601	4.098	10.932	4.054	11.889
G	2,750	1.762	2.199	24.801	2.011	14.132
G	3,000	1.010	1.250	23.762	1.071	6.040
SP-0.2 mmA	2,500	4.829	4.098	15.138	4.564	5.488
SP-0.35 mmA	2,500	5.861	4.098	30.080	5.771	1.536
SP-0.5 mmA	2,500	5.509	4.098	25.613	6.970	26.520
FPP-0.05 mmN	2,500	10	4.098	59.020	7.729	22.710
FPP-0.05 mmN	3,000	1.782	1.250	29.854	2.024	13.580
FPP-0.1 mmN	2,500	6.688	4.098	38.726	7.065	5.637
FPP-0.15 mmN	2,500	7.809	4.098	47.52	7.294	6.595
SF-30 min	2,500	10.000	4.098	59.020	8.960	10.400
SF-30 min	3,000	2.520	1.250	50.397	2.332	7.460
SP-0.35 mmA + SF-30 min	3,000	3.202	1.250	60.962	3.780	18.051

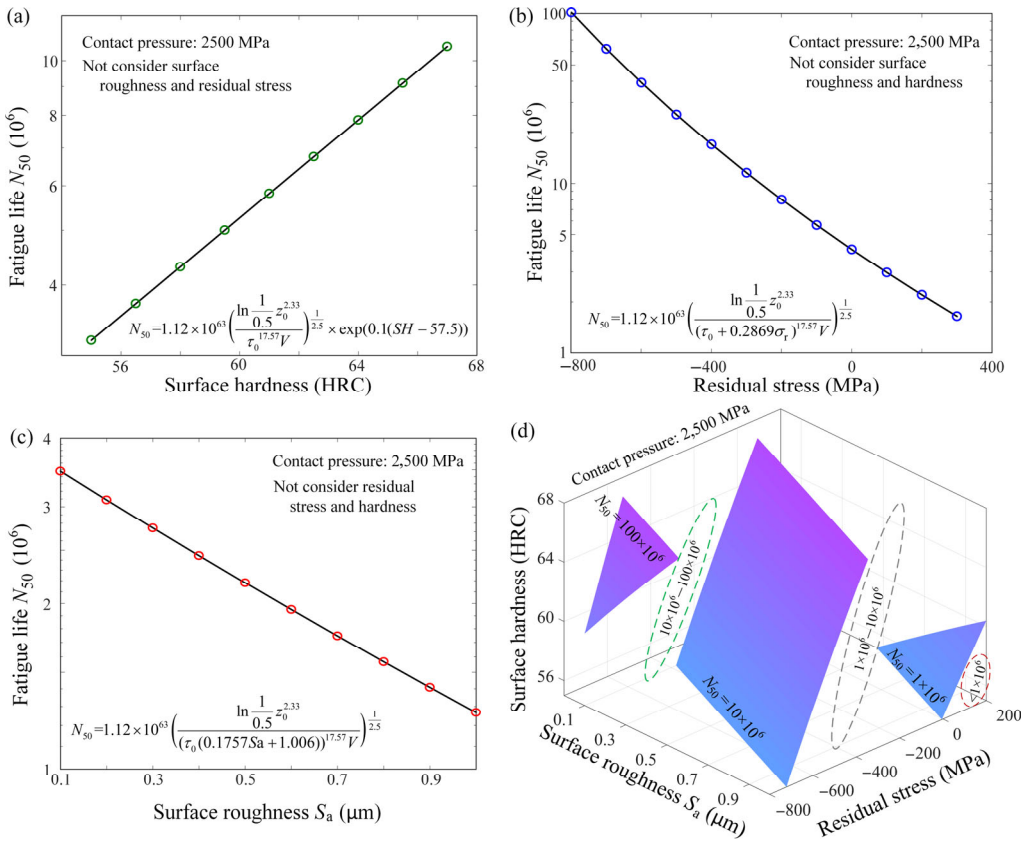

Fig. 12 Effect of (a) surface hardness, (b) residual stress on fatigue life, (c) surface roughness, and (d) surface hardness on fatigue life.

larger residual compressive stress at the maximum orthogonal shear stress depth can have longer fatigue life. Nevertheless, each surface strengthening technique displays certain limitations. For instance, the shot peening will lead to a more significant surface roughness while increasing the hardness and residual compressive stress [19, 59, 60]. The residual compressive stress layer of fine particle peening

and superfinishing is too shallow [61–63]. Therefore, combination strengthening methods will be a good choice. Firstly, the AISI 9310 components are treated with high-intensity shot peening to ensure sufficient residual compressive stress (> −400 MPa) at the depth of maximum orthogonal shear stress. After that, fine particle peening or superfinishing is applied to obtain a smaller roughness (< 0.15 μm). During this combined strengthening process, the surface hardness exceeds 62 HRC. Finally, the fatigue life of the AISI 9310 roller under 2,500 MPa can reach over 20×10^6 cycles.

5 Discussion

According to Fig. 11 and Table 7, this modified L–P fatigue model is able to give an accurate fatigue life assessment result for strengthened rollers in line contact. Gears are also in line contact during meshing. Thus, the possibility of the proposed method in gear application is discussed in Section 5.

For rollers and gears, the formulae of Hertz contact stress and contact half width are different due to their different geometric structures. Meanwhile, the values of exponents c, h, e, p, and A determined experimentally are also different. Therefore, Eqs. (8) and (9) cannot be used directly to assess the gear fatigue life. However, referring to the methods of Townsend and Zaretsky [42, 53], they multiplied some effect factors to Eq. (2) to consider the effects of the material and processing on fatigue life. We also multiply the surface integrity factors to Eq. (2), and then obtain Eq. (10). Then the ratio of predicted fatigue life N_1/N_2 of specimens after different surface strengthening processes can be calculated, as shown in Eq. (11). If the ratio of predicted fatigue life is similar to the ratio of experimental fatigue life, our modified L–P fatigue model can be applied to gears.

The modified L–P fatigue formula considering surface integrity can also be expressed as

$$N=\left(\frac{C_{\mathrm{D}}}{P_{\mathrm{d}}}\right)^{p}\left[\frac{\tau_0}{\tau_0(a_1S_{\mathrm{a}}+a_2)+a_3\sigma_{\mathrm{r}}}\right]^{d}\exp(m(SH-a_4)) \quad (10)$$

where the exponent d is typically selected as 9 [3].

The ratio of predicted fatigue lives of specimens under the same load condition and different surface integrity can be calculated by Eq. (11):

$$\frac{N_1}{N_2}=\left(\frac{\tau_0(a_1S_{\mathrm{a2}}+a_2)+a_3\sigma_{\mathrm{r2}}}{\tau_0(a_1S_{\mathrm{a1}}+a_2)+a_3\sigma_{\mathrm{r1}}}\right)^{9}\exp(0.1(SH_1-SH_2)) \quad (11)$$

where $a_1=0.1757$, $a_2=1.0060$, and $a_3=0.2869$. The S_{a1}, σ_{r1}, and SH_1 represent a set of surface integrity parameters of gears, and the N_1 is its predicted fatigue life. While the S_{a2}, σ_{r2}, and SH_2 represent another set of surface integrity parameters of gears, and the N_2 is its predicted fatigue life.

To assess the accuracy and possible application of Eq. (11) on gears, some literatures about the effect of the different surface strengthening methods on the fatigue life were referenced and discussed. Townsend and Zaretsky [53] conducted fatigue tests of two groups of carburized and hardened AISI 9310 gears under the maximum Hertz stress of 1,710 MPa. One gear group was manufactured with the standard ground tooth surface, while the second gear group was treated by shot peening after standard grinding. The surface hardness and core hardness of all gears were 58 and 40 HRC, respectively. The surface roughness, arithmetic mean height of contour lines R_{a} of all gears was 0.406 μm. The residual stress in the depth of the maximum orthogonal shear stress of the first and second groups were −186 and −260 MPa, respectively. The experimental results show that the fatigue life of shot-peened gear is 1.579 times that of the standard gears without shot peening. The ratio of predicted fatigue life of shot-peened gear to the standard gears without shot peening according Eq. (11) is equal to 1.619.

In Ref. [64], carburized and hardened AISI 9310 gears were ground with cubic boron nitride (CBN) or vitreous grinding mothed. The values of R_{a} of CBN and vitreous grinding gears were 0.091 and 0.139 μm, respectively. The values of surface hardness were 63 and 61.5 HRC, respectively. Although the residual stress in the depth of the maximum orthogonal shear stress was not given directly in his paper, these values of all gears could be estimated as −380 MPa (Fig. 4(a)). Then fatigue tests of two gear groups were carried out under the maximum Hertz stress of 1,710 MPa. The ratio of experimental fatigue life of CBN gear to vitreous grinding gears is 1.487, while the ratio

of predicted fatigue life is 1.282 according to Eq. (11). According to the data of these two papers, it can be found that the ratios of predicted fatigue life are close to the experimental life ratios. Therefore, Eq. (11) is also applicable to gears.

It means that if the fatigue life of gears in a state of surface integrity is known, then the fatigue life of other gears treated by a certain surface strengthening technique can be predicted based on Eq. (11).

6 Conclusions

Series of carburized AISI 9310 rollers with a variety of surface treatments were manufactured and tested. According to the results of surface integrity measurements and rolling contact fatigue tests, a modified rolling contact fatigue model was developed, which could consider surface integrity. Conclusions can be summarized as follows:

1) According to the rolling contact fatigue test results of AISI 9310 rollers under different loads, c and A appeared in the L–P model for AISI 9310 were determined as 17.57 and 1.12×10^{63}, respectively.

2) A modified L–P fatigue model considering surface integrity was proposed. Its predicted error of fatigue life was controlled in the 1.5 time of error band, in comparison to the experimental results. It can be an effective tool for estimating the contact fatigue life of strengthened specimens.

3) The method can be used to predict the contact fatigue life of gears indirectly. If the fatigue life of gears in a state of surface integrity is known, then the fatigue life of other gears treated by a certain surface strengthening techniques can be predicted based on the modified L–P fatigue model.

Acknowledgements

This work was supported the National Natural Science Foundation of China (No. 52275050) and Shaanxi Key Laboratory of Gear Transmission Open Program (No. SKLGT-2022-005).

Declaration of competing interest

The author has no competing interests to declare that are relevant to the content of this article.

References

[1] Weibull W. A statistical theory of the strength of materials. *Swed R Inst Eng Res* **151**: 1–45 (1939)

[2] Weibull W. The phenomenon of rupture in solids. *IVA Handlingar* **153** (1939)

[3] Lundberg G. Dynamic capacity of rolling bearings. *IVA Handlingar* **196** (1947)

[4] Lundberg G, Palmgren A. Dynamic capacity of rolling bearings. *J Appl Mech* **16**(2): 165–172 (1949)

[5] Ioannides E, Harris T A. A new fatigue life model for rolling bearings. *J Tribol* **107**(3): 367–377 (1985)

[6] Morris D, Sadeghi F, Chen Y C, Wang C, Wang B. Predicting material performance in rolling contact fatigue via torsional fatigue. *Tribol Trans* **62**(4): 614–625 (2019)

[7] Liu H L, Liu H J, Zhu C C, He H F, Wei P T. Evaluation of contact fatigue life of a wind turbine gear pair considering residual stress. *J Tribol* **140**(4): 041102 (2018)

[8] Shakoor M M, Ali M, Qamhiyah A, Flugrad D R. (2006) CAM size optimization based on a fatigue life model. In: Proceedings of the ASME 2006 International Design Engineering Technical Conferences and Computers and Information in Engineering Conference, Philadelphia, USA, 2006: 463–468.

[9] Zaretsky E V. Fatigue criterion to system design, life, and reliability. *J Propuls Power* **3**(1): 76–83 (1987)

[10] Cheenady A A, Arakere N K, Londhe N D. Accounting for microstructure sensitivity and plasticity in life prediction of heavily loaded contacts under rolling contact fatigue. *Fatigue Fract Eng M* **43**(3): 539–549 (2020)

[11] Li F K, Hu W P, Meng Q C, Zhan Z X, Shen F. A new damage-mechanics-based model for rolling contact fatigue analysis of cylindrical roller bearing. *Tribol Int* **120**: 105–114 (2018)

[12] CH-ISO. ISO 281 Rolling bearings—Dynamic load ratings and rating life. ISO, 2007.

[13] Wu J Z, Wei P T, Liu H J, Zhang B Y, Tao G B. Effect of shot peening intensity on surface integrity of 18CrNiMo7–6 steel. *Surf Coat Tech* **421**: 127194 (2021)

[14] Lin Q J, Liu H J, Zhu C C, Parker R G. Investigation on the effect of shot peening coverage on the surface integrity. *Appl Surf Sci* **489**: 66–72 (2019)

[15] Liu G, Lu J, Lu K. Surface nanocrystallization of 316L stainless steel induced by ultrasonic shot peening. *Mater Sci Eng A* **286**(1): 91–95 (2000)

[16] Child D J, West G D, Thomson R C. Assessment of surface hardening effects from shot peening on a Ni-based alloy using electron backscatter diffraction techniques. *Acta Mater* **59**(12): 4825–4834 (2011)

[17] Wu J Z, Liu H J, Wei P T, Lin Q J, Zhou S S. Effect of shot peening coverage on residual stress and surface roughness of 18CrNiMo7–6 steel. *Int J Mech Sci* **183**: 105785 (2020)

[18] Kobayashi M, Matsui T, Murakami Y. Mechanism of creation of compressive residual stress by shot peening. *Int J Fatigue* **20**(5): 351–357 (1998)

[19] Bagherifard S, Guagliano M. Fatigue behavior of a low-alloy steel with nanostructured surface obtained by severe shot peening. *Eng Fract Mech* **81**: 56–68 (2012)

[20] Unal O, Varol R. Surface severe plastic deformation of AISI 304 via conventional shot peening, severe shot peening and repeening. *Appl Surf Sci* **351**: 289–295 (2015)

[21] Lee S Y, Ling J J, Wang S H, Ramirez-Rico J. Precision and accuracy of stress measurement with a portable X-ray machine using an area detector. *J Appl Cryst* **50**(1): 131–144 (2017)

[22] Lin Q J, Liu H J, Zhu C C, Chen D F, Zhou S S. Effects of different shot peening parameters on residual stress, surface roughness and cell size. *Surf Coat Tech* **398**: 126054 (2020)

[23] Zhang X H, Liu H J, Wu S J, Li G M, Wei P T. Experimental investigation on the effect of barrel finishing processes on surface integrity of 18CrNiMo7–6 carburized rollers. *P I Mech Eng E-J Pro* **236**(5): 2095–2105 (2022)

[24] Ohta T, Ma N S. Shot velocity measurement using particle image velocimetry and a numerical analysis of the residual stress in fine particle shot peening. *J Manuf Process* **58**: 1138–1149 (2020)

[25] Lundberg G, Palmgren A. Dynamic capacity of roller bearings. *Acta Polytechnica* **2**(4): 96–127 (1952)

[26] Palmgren A. *Ball and Roller Bearing Engineering*. Philadelphia (USA): SKF Industries Inc., 1959.

[27] Zaretsky E V, Parker R J, Anderson W J, Miller S T. Effect of component differential hardness on residual stress and rolling-contact fatigue. In: NASA Technical Note, Cleveland, USA, 1965: NASA-TN-D-2664.

[28] Zaretsky E V, Parker R J, Anderson W J. Effect of component differential hardnesses on rolling-contact fatigue and load capacity. In: NASA Technical Note, Cleveland, USA, 1965: NASA-TN-D-2640.

[29] Zaretsky E V. Selection of rolling-element bearing steels for long-life application. In: NASA Technical Memorandum, Cleveland, USA, 1986: NASA-TM-88881.

[30] Zaretsky E V. Rolling bearing life prediction, theory, and application. In: NASA Technical Publication, Cleveland, USA, 2013: NASA/TP-2013-215305.

[31] Moyar G J, Sharma V. Orthogonal shear stress amplitude as a function of rolling contact ellipticity and depth. *J Tribol* **119**(4): 883–886 (1997)

[32] Johnson K L. *Contact Mechanics*. Cambridge (UK): Cambridge University Press, 1987.

[33] Coy J J. Analysis of dynamic capacity of low-contact-ratio spur gears using Lundberg–Palmgren theory. In: NASA Technical Note, Cleveland, USA, 1975: NASA-TN-D-8029.

[34] Townsend D P, Coy J J, Zaretsky E V. Experimental and analytical load-life relation for AISI 9310 steel spur gears. *J Mech Design* **100**(1): 54–60 (1978)

[35] Coy J J, Townsend D P, Zaretsky E V. An update on the life analysis of spur gears. *Adv Power Trans Tech*: 421–433 (1983)

[36] Govindarajan N, Gnanamoorthy R. Rolling/sliding contact fatigue life prediction of sintered and hardened steels. *Wear* **262**(1–2): 70–78 (2007)

[37] Liu C R, Choi Y. Rolling contact fatigue life model incorporating residual stress scatter. *Int J Mech Sci* **50**(12): 1572–1577 (2008)

[38] Choi Y. A study on the effects of machining-induced residual stress on rolling contact fatigue. *Int J Fatigue* **31**(10): 1517–1523 (2009)

[39] Choi Y, Liu C R. Rolling contact fatigue life of finish hard machined surfaces Part 1. Model development. *Wear* **261**(5–6): 485–491 (2006)

[40] Walvekar A A, Sadeghi F. Rolling contact fatigue of case carburized steels. *Int J Fatigue* **95**: 264–281 (2017)

[41] Wang W, Liu H J, Zhu C C, Tang J Y, Jiang C X. Evaluation of contact fatigue risk of a carburized gear considering gradients of mechanical properties. *Friction* **8**(6): 1039–1050 (2020)

[42] Zaretsky E V. Rolling bearing steels—A technical and historical perspective. *Mater Sci Technol* **28**(1): 58–69 (2012)

[43] Ne'lias D, Dumont M L, Champiot F, Vincent A, Girodin D, Fouge'res R, Flamand L. Role of inclusions, surface roughness and operating conditions on rolling contact fatigue. *J Tribol* **121**(2): 240–251 (1999)

[44] Ås S K, Skallerud B, Tveiten B W. Surface roughness characterization for fatigue life predictions using finite element analysis. *Int J Fatigue* **30**(12): 2200–2209 (2008)

[45] Lai J B, Huang H Z, Buising W. Effects of microstructure and surface roughness on the fatigue strength of high-strength steels. *Procedia Struct Integr* **2**: 1213–1220 (2016)

[46] Zhang B Y, Liu H J, Zhu C C, Ge Y B. Simulation of the fatigue-wear coupling mechanism of an aviation gear. *Friction* **9**(6): 1616–1634 (2021)

[47] Zhang B Y, Liu H J, Zhu C C, Li Z M Q. Numerical simulation of competing mechanism between pitting and micro-pitting of a wind turbine gear considering surface roughness. *Eng Fail Anal* **104**: 1–12 (2019)

[48] Bergstedt E, Lin J C, Olofsson U. Influence of gear surface roughness on the pitting and micropitting life. *P Inst Mech Eng C-J Mec* **234**(24): 4953–4961 (2020)

[49] Morales-Espejel G E, Gabelli A, de Vries A J C. A model for rolling bearing life with surface and subsurface survival—Tribological effects. *Tribol Trans* **58**(5): 894–906 (2015)

[50] Balan M R, Tufescu A, Cretu S S. A case study on relation between roughness, lubrication and fatigue life of rolling bearings. *IOP Conf Ser Mater Sci Eng* **147**: 012013 (2016)

[51] Leibensperger R L, Brittain T M. Shear stresses below asperities in Hertzian contact as measured by photoelasticity. *J Lubr Tech* **95**(3): 277–283 (1973)

[52] Zhou R S. Surface topography and fatigue life of rolling contact bearing. *Tribol Trans* **36**(3): 329–340 (1993)

[53] Townsend D P, Zaretsky E V. Effect of shot peening on surface fatigue life of carburized and hardened AISI 9310 spur gears. *J Aerospace* **97**(1): 807–818 (1988)

[54] Agha S R. Fatigue performance of superfinish hard turned surfaces in rolling contact. Ph.D. Thesis. West Lafayette (USA): Purdue University, 2000.

[55] Bernasconi A, Davoli P, Filippini M, Foletti S. An integrated approach to rolling contact sub-surface fatigue assessment of railway wheels. *Wear* **258**(7–8): 973–980 (2005)

[56] Wang W, Liu H J, Zhu C C, Bocher P, Liu H L, Sun Z D. Evaluation of rolling contact fatigue of a carburized wind turbine gear considering the residual stress and hardness gradient. *J Tribol* **140**(6): 061401 (2018)

[57] Shalabi M M, Gortemaker A, Van't Hof M A, Jansen J A, Creugers N H J. Implant surface roughness and bone healing: A systematic review. *J Dent Res* **85**(6): 496–500 (2006)

[58] Nwaogu U C, Tiedje N S, Hansen H N. A non-contact 3D method to characterize the surface roughness of castings. *J Mater Process Tech* **213**(1): 59–68 (2013)

[59] Vrbka M, Křupka I, Svoboda P, Šperka P, Návrat T, Hartl M, Nohava J. Effect of shot peening on rolling contact fatigue and lubricant film thickness within mixed lubricated non-conformal rolling/sliding contacts. *Tribol Int* **44**(12): 1726–1735 (2011)

[60] Seki M, Soyama H, Kobayashi Y, Gowa D, Fujii M. Rolling contact fatigue life of steel rollers treated by cavitation peening and shot peening. *J Solid Mech Mater Eng* **6**(6): 478–486 (2012)

[61] Zhang B Y, Wei P T, Liu H J, Yan H, Guagliano M. Effect of fine particle peening on surface integrity of flexspline in harmonic drive. *Surf Coat Tech* **433**: 128133 (2022)

[62] Oguri K. Fatigue life enhancement of aluminum alloy for aircraft by Fine Particle Shot Peening (FPSP). *J Mater Process Tech* **211**(8): 1395–1399 (2011)

[63] Morita T, Noda S, Kagaya C. Influences of fine-particle bombarding and conventional shot peening on surface properties of steel. *Mater Trans* **55**(4): 646–652 (2014)

[64] Townsend D P, Patel P R. Surface fatigue life of CBN and vitreous ground carburized and hardened AISI 9310 spur gears. *J Aerospace* **97**(1): 819–827 (1988)

Boyu ZHANG. She has been studying as a doctoral student in the State Key Laboratory Mechanical Transmissions (SKLMT), Chongqing University, China, since 2020. Her research interest includes gear contact fatigue and shot peening enhancement.

Huaiju LIU. He is currently a professor in the State Key Laboratory of Mechanical Transmissions (SKLMT), Chongqing University, China. He received his Ph.D. degree from the University of Warwick, UK, in 2013. His research fields include tribology and fatigue behaviors of mechanical elements.

Peitang WEI. He is currently working as an associate professor in the State Key Laboratory of Mechanical Transmissions (SKLMT), Chongqing University, China. He received his Ph.D. degree from University of Wollongong, Australia. His research fields include gear fatigue mechanism, crystal plasticity modeling, and gear testing.

Mario GUAGLIANO. He is a full professor in machine design, Polytechnic University of Milan, Italy. He is a vice president of the 14th International Shot Peening Conference. His main scientific interests are innovative methods for mechanical design, shot peening, kinetic treatments and coating techniques for surface functionalization and for superior properties as well as to obtain nanostructured surfaces.

Shengwen HOU. He is an engineer in Shaanxi Fast Auto Drive Refco Group Ltd., China. He is mainly engaged in gear drive design.